https://doi.org/10.5194/acp-2021-884
Preprint. Discussion started: 25 November 2021

Atmospheric Chemistry and Physics Discussions
Open Access

Would El Niño enhance or suppress the migrating diurnal tide in the MLT region?

Yetao Cen[1,2,3], Chengyun Yang[1,2,3*], Tao Li[1,2,3*], Jia Yue[5,6], James M. Russell III[6], and Xiankang Dou[1,2,3,4]

[1]CAS Key Laboratory of Geospace Environment, School of Earth and Space Sciences, University of Science and Technology of China, Hefei, Anhui, China

[2]Mengcheng National Geophysical Observatory, School of Earth and Space Sciences, University of Science and Technology of China, Hefei, Anhui, China

[3]CAS Center for Excellence in Comparative Planetology, University of Science and Technology of China, Hefei, Anhui, China

[4]School of Electronic Information, Wuhan University, Wuhan, Hubei, China

[5]Catholic University of America, DC, USA

[6]Center for Atmospheric Sciences, Hampton University, Hampton, VA, USA

Correspondence: Chengyun Yang (cyyang@ustc.edu.cn) and Tao Li (litao@ustc.edu.cn)

https://doi.org/10.5194/acp-2021-884
Preprint. Discussion started: 25 November 2021

Atmospheric Chemistry and Physics Discussions
Open Access

Abstract

Previous observations and simulations are controversial as to whether El Niño will increase or decrease the diurnal tide (DW1) in the upper mesosphere and lower thermosphere (MLT) region. This study revisited the linear response of the MLT DW1 to El Niño during the winter (December-January-February) based on 19-year satellite observations of Sounding of the Atmosphere using Broadband Emission Radiometry (SABER). The MLT DW1 temperature amplitudes decreased by ~10% during four El Niño winters from 2002 to 2020, consistent with the results from the simulation of the Specified-Dynamics version of the Whole Atmosphere Community Climate Model (SD-WACCM). According to the multiple linear regression analysis, the linear effects of El Niño-Southern Oscillation (ENSO) on tropical MLT DW1 are negative in both SABER observations and SD-WACCM simulations. In the SD-WACCM simulation, Hough mode (1, 1) dominates the DW1 tidal variation in the tropical MLT region. The consistency between the (1, 1) mode in the tropopause region and in the MLT region, as well as the downward phase progression from 15 to 100 km, indicates the direct upward propagation of DW1 from the excitation source in the troposphere. During 7 of 8 El Niño winters from 1979 to 2014, the anomalous amplitudes of the (1, 1) mode are negative in both the tropopause region and MLT region. The suppressed DW1 heating rates in the tropical troposphere (average over ~0-16 km and 35°S-35°N) during the El Niño events contribute to the decreased DW1 tide. The mesospheric latitudinal zonal wind shear anomalies during El Niño winters would lead to a narrower waveguide and prevent the vertical propagation of the DW1 tide. The gravity wave drag excited by convection also plays a role in modulating the MLT DW1 amplitude.

https://doi.org/10.5194/acp-2021-884
Preprint. Discussion started: 25 November 2021

1 Introduction

Atmospheric solar tides are global-scale variations in meteorological variables (e.g., density, wind, and temperature) with subharmonic periods of a solar day. The migrating diurnal tide is dominant in the tropical mesosphere and lower thermosphere (MLT) region and is characterized by westward travelling zonal wavenumber 1, hereafter denoted as DW1 (Chapman & Lindzen, 1970). DW1 is primarily excited by the absorption of infrared (IR) radiation by water vapour in the troposphere (~0–15 km) (Hagan et al., 2002) and can propagate vertically and reach maximum amplitude in the MLT region (Walterscheid., 1981a; McLandress., et al., 1996; Liu & Hagan, 1998; Lu et al., 2009; Liu et al., 2010; Yang et al., 2018). Diurnal migrating tides remain a significant focus of scientific research due to a lack of comprehensive understanding of their seasonal and interannual variabilities. The tidal variation in the MLT region depends on variations in the wave sources, such as the solar heating absorption in the lower atmosphere (Chapman & Lindzen, 1970), and the tidal wave propagation, which is affected by background wind variation, such as the QBO (Forbes and Vincent, 1989; Hagan et al., 1999; McLandress, 2002b; Ramesh et al., 2020; McLandress, 2002; Mayr and Mengel, 2005). In addition to tidal sources and propagation, tidal variability is also affected by the modulation of interactions with gravity waves (GW) (Liu and Hagan, 1998; Li et al., 2009).

As the dominant interannual variation in the tropical troposphere (Yulaeva and Wallace, 1994), the El Niño-Southern Oscillation (ENSO), which is characterized by anomalous sea surface temperature in the eastern equatorial Pacific Ocean, can cause global-scale perturbations in atmospheric temperature, rainfall, and cloudiness and potentially modulate tidal heating sources in the troposphere (Lieberman et al., 2007). Previous studies have documented that ENSO can influence the troposphere (Yulaeva and Wallace, 1994; Calvo-Fernandez et al., 2004) and the stratosphere and mesosphere (Sassi et al., 2004; Randel et al., 2009; Li et al., 2013 and 2016). As ENSO events tend to reach their maximum in the Northern Hemisphere winter, they could potentially significantly impact the MLT tide.

https://doi.org/10.5194/acp-2021-884
Preprint. Discussion started: 25 November 2021

Atmospheric Chemistry and Physics Discussions

According to meridional wind observations from the meteor radar at Jakarta (6.4°S, 106.7°E) and medium-frequency (MF) radar at Tirunelveli (8.7°N, 77.8°E), the tropical diurnal tidal amplitudes in the meridional winds were suppressed during the El Niño winters of 1994/1995 and 1997/1998 (Gurubaran et al., 2005). However, Lieberman et al. (2007) documented a dramatic enhancement of the equatorial diurnal tide during 1997 based on MF radar observations at Kauai, Hawaii (22°N, 154°W), which may be connected to more substantial solar heating absorbed by water vapour during the strong El Niño event of 1997-1998. Notably, the positive diurnal tidal amplitude anomaly became much weaker during the wintertime of 1997/1998 when El Niño reached its maximum. In addition, the diurnal tidal amplitudes were suppressed rather than enhanced during the winters of another 3 El Niño events (1991/1992, 1994/1995, and 2002/2003). From July to October of the strong El Niño of 2015, the equatorial DW1 in the MLT was dramatically enhanced, as observed by ground-based radars and the Thermosphere Ionosphere Mesosphere Energetics and Dynamics (TIMED)/SABER satellite (Zhou et al., 2018; Kogure et al., 2021). Similar to the strong El Niño of 1997-1998 (Lieberman et al., 2007), the positive anomaly of the diurnal tide amplitude also became much weaker (Zhou et al., 2018) or even negative (Kogure et al., 2021) in winter.

Utilizing the Whole Atmosphere Community Climate Model (WACCM) version 4, Pedatella & Liu (2012 and 2013) suggested that El Niño could enhance the MLT DW1 tide during winters due to increased tropospheric radiative forcing. In their simulation, the QBO signal is not included, and the ENSO events are self-generated. As suggested by the WACCM version 6 simulations with self-generated QBO and ENSO, there is a positive response of the MLT DW1 tide to El Niño during the winter (Ramesh et al., 2020). However, Liu et al. (2017) found that DW1 amplitudes are suppressed during the winters of El Niño events based on simulations of the ground-to-topside atmosphere-ionosphere for aeronomy (GAIA) model. Since GAIA is nudged with reanalysis data below 30 km, ENSO events and variations in the lower atmosphere are more realistic. The discrepancies among the model simulations and

https://doi.org/10.5194/acp-2021-884
Preprint. Discussion started: 25 November 2021

uncertainties in the observations require further investigation of the DW1 tide-ENSO connection.

The response of the MLT DW1 tide to ENSO during the winters is revisited in this study based on the DW1 variation extracted from a long-term temperature dataset observed by the Sounding of the Atmosphere using Broadband Emission Radiometry (SABER) onboard the TIMED (Mertens et al., 2001, 2004, Rezac et al. 2015). The "Specified-Dynamics" version of the WACCM simulation is used to study the possible mechanism. The data and methods are described in section 2. Section 3 presents the observational and model results of the DW1 temperature response to ENSO. In section 4, we examine the possible mechanism that modulates the MLT DW1 tide during ENSO events. Finally, a summary is presented in section 5.

2 Data and Methods

The SABER onboard the TIMED satellite began its observations in January 2002. Kinetic temperature profiles are retrieved from the CO2 limb emission profiles from the tropopause to the lower thermosphere using a full non-LTE inversion (Mertens et al., 2001, 2004, Rezac et al. 2015). The latitude range of SABER observations is from 53° in one hemisphere to 83° in the other, and the latitude coverage flips to the opposite hemisphere approximately every 60 days. Thus, SABER provides nearly continuous soundings within 53°S and 53°N. This study used version 2.0 temperature data from February 2002 through July 2021 to analyse the DW1 temperature tide in the MLT region. The SABER can complete a nearly 24-hr local time observation within an ~60-day window, which allows us to extract the diurnal tide explicitly.

The method described by Xu et al. (2007) is utilized to extract the DW1 tide from TIMED/SABER temperature data. Migrating tides can be expressed as

$$\frac{1}{2\pi}\int_0^{2\pi} T(t_{LT},\lambda)d\lambda = \overline{T}(t_{LT}) + \sum_{n=1}^{N} T_n^{mtw}\cos\left(n\omega_0 + \psi_n^{mtw}\right) + T_{r1} \qquad (1)$$

where T is temperature, t_{LT} is local time, λ is longitude, $\overline{T}$ is zonal mean

https://doi.org/10.5194/acp-2021-884
Preprint. Discussion started: 25 November 2021

temperature, $\sum_{n=1}^{N} T_n^{mtw} \cos(n\omega_0 + \psi_n^{mtw})$ is migrating tides, and T_{r1} is remnant. To extract tidal components, the daily data are first divided into two groups by local time corresponding to the ascending and descending phases, and then, each group is interpolated into 12 longitude grids, each 30° wide, by fitting with a cubic spline. The next step is to calculate the zonal mean for each day to eliminate the nonmigrating tides as well as the stationary planetary waves. The bimonthly amplitudes and phase information of the migrating tides can be calculated by nonlinear least-squares fitting techniques using data within a 60-day sliding window every month (Xu et al., 2007; Smith et al., 2012; Gan et al., 2014).

The WACCM is a fully coupled chemistry-climate model, which is the high-top atmosphere component of the Community Earth System Model (CESM) (Garcia et al., 2007). In this study, the simulation of the Specified-Dynamics (SD) version of WACCM (SD-WACCM), version 4 is adopted to investigate the ENSO-DW1 tide relationship. The vertical range of SD-WACCM extends from the surface up to ~140 km. The simulated diurnal tide in WACCM4 compares favourably with observations (Lu et al., 2011; Davis et al., 2013). SD-WACCM is nudged to meteorological fields from Modern-Era Retrospective Analysis for Research and Applications (MERRA) reanalysis data in the troposphere and stratosphere (from the surface up to 1 hPa) and then is freely run in the MLT (above 0.3 hPa) (Kunz et al., 2011). Smith et al. (2017) discussed the dynamic constraints in SD-WACCM and their impact on simulation of the mesosphere in detail. The ENSO-related characteristics in the troposphere and stratosphere in SD-WACCM follow those in the reanalysis meteorological fields with relaxation. In this study, the SD-WACCM output includes complete diurnal tidal information for temperature, zonal and meridional wind, and heating processes from 1979 to 2014. The simulation also outputs the diurnal components of parameterized GW drag.

The Niño3.4 index (N3.4), which is the sea surface temperature (SST) anomaly averaged over 120°-170°W and 5°S-5°N (available at https://www.esrl.noaa.gov/psd/gcos_wgsp/Timeseries/Data/Niño34), is used to

https://doi.org/10.5194/acp-2021-884
Preprint. Discussion started: 25 November 2021

Atmospheric Chemistry and Physics Discussions

identify El Niño and La Niña events.

The monthly DW1 can be used as a vector with the ratio as the amplitude and the angle as the phase. To evaluate the variations in both the amplitude and phase of the DW1 tide, the monthly DW1 amplitudes are weighted by projecting the monthly mean vectors onto the climatological mean DW1 vector with the phase difference cos ($\Delta\varphi$) (the phase difference is $\Delta\varphi=\varphi-\varphi_{clim}$) as follows:

$$\mathrm{Amp_{weighted}} = \mathrm{Amp} * \cos\left(\omega * \left(\varphi - \varphi_{clim}\right)\right) \quad (2)$$

where ω ($\omega=2\pi/24$) is the frequency of the DW1 tide. φ and φ_{clim} are the DW1 phase of each month and the climatological mean, respectively. In the remainder of this study, the weighted DW1 amplitude (and its anomaly) refer to the DW1 amplitude (anomaly) for conciseness. The mean tidal amplitude and phase during northern winter are derived from the averaged tidal vectors for December, January, and February (DJF) of each year.

To derive the winter interannual variability that may be related to ENSO, we first calculate the DW1 anomalies by removing the climatological mean seasonal cycle. Then, the winter (DJF) mean of the DW1 anomalies is calculated. Natural forcing, such as the solar cycle (represented by F107), QBO, ENSO, and long-term trends, jointly affect the DW1 tidal amplitude (e.g., Dhadly et al., 2018; Gurubaran et al., 2005; Gurubaran & Rajaram, 1999; Hagan et al., 1999; Lieberman et al., 2007; Liu et al., 2017; Pedatella & Liu, 2012; Sridharan, 2019, 2020; Sridharan et al., 2010; Vincent et al., 1998; Xu et al., 2009). To isolate the linear forcing of ENSO from the interference of other factors, a multivariate linear regression (MLR) analysis is applied on the anomalous time series at each latitude and altitude, the same as that used in Li et al. (2013).

$$\mathrm{T(t)} = \mathrm{C_1} * \mathrm{NIÑO3.4} + \mathrm{C_2} * \mathrm{QBO10} + \mathrm{C_3} * \mathrm{QBO30} + \mathrm{C_4} * \mathrm{F107} + \mathrm{C_5} * \mathrm{TREND} + \varepsilon(\mathrm{t}) \quad (3)$$

where T is the DW1-T anomaly, t is time, C1–C5 are regression coefficients, and

https://doi.org/10.5194/acp-2021-884
Preprint. Discussion started: 25 November 2021

ε is the residual; QBO10 and QBO30 are two orthogonal QBO time series derived from the zonal wind (m s^{-1}) averaged over 5°N to 5°S at 10 and 30 hPa (Wallace et al., 1993), respectively. The Niño3.4 index (NIÑO3.4) is the 3-month running mean of SST averaged over 5°N to 5°S, 120°W-170°W; F107 is the solar radio flux at 10.7 cm, which is a proxy for solar activity; and TREND is the long-term linear trend. The linear contribution of each factor during winters is determined by applying MLR to DJF anomalies each year. The analysis is carried out for the period of 2002–2020 at each latitude and pressure grid point. The F test (Kissell et al., 2017) was used to evaluate the statistical significance of the regression coefficients.

The Hough function in classic tidal theory (Lindzen and Chapman, 1969), which represents the solution of the Laplace tide equation in the isothermal atmosphere, can set a consistent latitude variation in the amplitude and phase of the tidal perturbation field. The Hough functions of daily variation frequency form a complete orthogonal set and extend from 90°S to 90°N. This method of estimating amplitude and phase is based on fitting the Hough mode to the zonal structure representation and the simple harmonic function (sine and cosine) to the local time-varying representation. The Hough mode is represented as $\Theta_{s,n}(\theta)$, or (s, n), where s indicates the zonal wavenumber and index n is positive for gravitational modes (propagating modes) and negative for rotational modes (trapped modes). The normalized functions satisfy the following relation

$$\int_{-90^\circ}^{90^\circ}\Theta_{1,n}(\theta)\bullet\Theta_{1,m}(\theta)\cos(\theta)d\theta=\begin{cases}1, m=n\\0, m\neq n\end{cases}, n,m=\pm1,\pm2,... \qquad (4)$$

3 Results

Figures 1a and 1b show the monthly mean DW1 temperature amplitude anomalies (removing the climatological mean seasonal cycle) averaged over

https://doi.org/10.5194/acp-2021-884
Preprint. Discussion started: 25 November 2021

10°S-10°N at 100 km derived from SABER observations and SD-WACCM simulations between 2002 and 2020, respectively. Among the analysed period, there were 4 El Niño events in 2002, 2006, 2009, and 2015, which are indicated with red arrows and defined by the Niño3.4 index in Figure 1c; the 3 La Niña events in 2007, 2010, and 2020 are indicated with blue arrows. The anomalous DW1 amplitudes are negative during 4 El Niño winters and positive during all 3 La Niña events. The DW1 anomalies reach a positive maximum in July to October during the 2015/2016 strong El Niño event, which agrees with Zhou et al. (2020); however, they become negative in winter. In the period when SD-WACCM and SABER overlap (2002-2014), the simulated DW1 amplitude anomalies in SD-WACCM are negative during all 3 El Niño winters (2002, 2006, and 2009) and positive during 2 La Niña events. The negative response of the MLT DW1 tide to El Niño in the SD-WACCM simulation agrees well with that in the SABER observation.

In the 35-yr SD-WACCM simulations (1979-2014), the anomalous DW1 amplitudes averaged over 10°S-10°N at 100 km are negative during 7 of 8 El Niño winters (1982, 1986, 1991, 1997, 2002, 2006, and 2009), as shown in Table 1. The MLR coefficients of DW1 to normalized Niño3.4 are significantly negative in both the SABER observation and SD-WACCM simulation, as shown in Figure 2. The MLR coefficients of tropical DW1 to Niño3.4 in the SABER observation (with a minimum of ~-1 K/index) are twice as strong as those (with a minimum of ~-0.5 K/index) in the SD-WACCM simulation since the magnitude of the DW1 tide is underestimated in the WACCM4 simulation (Liu 2010; Lu et al., 2012). The negative response of the MLT DW1-T amplitude to El Niño is consistent with early MF radar/meteor radar observations and GAIA model simulations with a nudging process (Gurubaran, 2005 and Liu et al., 2017) but opposite to free-run WACCM simulations (Pedatella & Liu 2012 and 2013).

The MLR coefficients of the DW1 response to normalized QBO10 and QBO30 in the equatorial mesopause region are significantly positive, with a minimum of ~1

https://doi.org/10.5194/acp-2021-884
Preprint. Discussion started: 25 November 2021

K/(m*s^{-1}) near 100 km (Figure S1), consistent with previous studies (Ramesh et al. 2021). The linear effects of the QBO on the MLT DW1 tides are comparable to those of ENSO (the variances in the DW1 tide explained by ENSO, QBO10, and QBO30 are 23%, 20%, and 17%, respectively). The interaction between the QBO and ENSO may potentially modulate the ENSO-DW1 tide relationship (Grey, 1988). In this study, we focused on the linear effect of ENSO on the MLT DW1 tidal variability and the associated mechanism. In SD-WACCM, the linear regression coefficients of DW1 are a negative response to Niño3.4 and a positive response to QBO10 and QBO30, which is consistent with the SABER observation, although the absolute value of the coefficients decreases more than that of SABER. The variance percentages of F107 are negligible compared with these three variables. In the remainder of this study, only the linear effect of ENSO on the MLT DW1 tide is discussed.

https://doi.org/10.5194/acp-2021-884
Preprint. Discussion started: 25 November 2021

4 Possible Mechanisms

4.1 Tidal forcing and propagation

A specific tidal component, such as DW1, can be decomposed into a series of gravity wave-like modes and Rossby wave-like modes based on the Hough functions (Figure S2) (Auclair-Desrotour et al., 2017; Chapman & Lindzen, 1970; Forbes, 1995). In a qualitative sense, the tidal response can be considered a combination of GWs restored by stable stratification and inertial Rossby waves due to Coriolis acceleration. The Hough modes of the DW1 tide in the SD-WACCM simulation are analysed to examine the mechanism of tropical DW1 tidal variation. As shown in Figure 3a, the anomalies of the DW1 temperature amplitude averaged over 10°S-10°N at 100 km are consistent with its Hough (1,1) component (the correlation coefficient between MLT DW1-T anomalies and its Hough (1,1) component is 0.99) during the Northern Hemisphere (NH) winter from 1979 to 2013. The DW1-T amplitude anomalies and their Hough (1,1) component during El Niño years decrease by 15% compared to the climatological mean amplitude. During winters (DJF) from 1979 to 2013, the average phase of DW1-T over 10°S-10°N shows general downward phase progression with the height from the MLT region to the tropopause region (approximately 15 km). This kind of downward phase advance with height implies an upward group velocity for the vertically propagating gravity model. By tracking the downward phase progressive line, the altitude of the excitation source is estimated to be below 15 km. The DW1-T phase during El Niño winters corresponds with the climatological mean phase structure, implying that ENSO-induced tidal perturbation in the troposphere could directly propagate vertically into the MLT region. The anomalous Hough (1,1) mode of the DW1 temperature amplitude at MLT (100 km) is significantly correlated (the correlation coefficient is 0.81) with that at the tropopause region (15 km), indicating the effective propagation of the perturbation in the tropospheric Hough (1,1) into the MLT region. During 7 of 8 El Niño events (1982, 1986, 1991, 1997, 2002, 2006, and 2009), the Hough (1,1) mode at 100 km is ~10%

smaller than that in the tropopause, which agrees well with the suppressed Hough (1,1) in the MLT.

As noted earlier, the DW1 tide is primarily excited by the absorption of solar radiation by tropospheric water vapour (Lieberman et al., 2003; Zhang et al., 2010). According to the tidal theory (Volland and Hans, 1988), the heating rate of radiation absorbed by water vapour in the entire troposphere is responsible for the excitation of diurnal migrating tides. Next, we examine the perturbation of the DW1 solar heating source in the SD-WACCM simulation, which potentially contributes to the negative Hough (1,1) tidal anomalies in the tropopause region during El Niño winters. As presented in Figure 4, the anomalous amplitudes of the DW1 heating rate (HR) regressed on the normalized Niño3.4 index are significantly positive (with a maximum of ~0.4 mW/m^3 per index) in the upper tropical troposphere (5°S-5°N, 3-12 km) but are significantly negative below 3 km (with a minimum of ~-4 mW/m^3 per index). The ENSO-induced changes in the tropospheric DW1 heating forcing may be due to the redistribution of tropospheric convection during El Niño and La Niña winters. During El Niño winters, increased moisture in the upper troposphere due to enhanced tropical precipitation in the central Pacific Ocean (e.g., Hoerling et al., 1997) leads to stronger solar heating absorption by water vapour in the middle and upper equatorial troposphere (5–12 km, 10°S–10°N). On the other hand, heating in the lower troposphere significantly decreased due to less solar radiation below the convective cloud. The DW1 HR regressed on Niño3.4 in the NH (5°N-35°N) is characterized by a significantly negative coefficient of 3-8 km (with a maximum of ~-0.3 mW/m^3 per index) associated with significantly positive coefficients below 2 km (with a maximum of ~3 mW/m^3 per index). In the Southern Hemisphere, the distribution of DW1 HR coefficients consists of negative and positive values at different altitudes and latitudes.

Pedatella et al. (2013) adopted the HR in the upper tropical troposphere (5-10 km within ±20°) to estimate the ENSO-induced variation in the DW1 tidal source. Other

https://doi.org/10.5194/acp-2021-884
Preprint. Discussion started: 25 November 2021

studies suggested the HR in both the upper and lower troposphere (e.g., altitude range between 900-200 hPa, 1-12 km in Lieberman et al., 2003, and 1000-100 hPa, 0-16 km in Zhang et al., 2010). As suggested by Table 2, the mass-weighted HR averaged over the entire tropical troposphere (0-16 km, 35°N-35°S), which negatively responds to ENSO, is significantly correlated (the correlation coefficient is 0.45) with the DW1 tide in the tropical tropopause region. The HR averaged over 5-10 km, 20°N-20°S (the same as in Pedatella et al., 2013) regressed on Niño3.4 is also negative, although it is not significantly correlated with the DW1 tidal variation in the tropopause. The decreased DW1 heating source in the troposphere during El Niño is a primary cause of the suppressed DW1 tide in the tropopause region winters, which propagates vertically and affects the DW1 tidal variation in the MLT region.

4.2 Effect of background wind

The zonal wind in the middle atmosphere can modulate tide propagation from the troposphere to the MLT (Forbes and Vincent, 1989). As Mclandress (2002) described, the perturbation latitudinal shear in the zonal mean zonal wind (zonal mean vorticity) can affect DW1 propagation into the MLT region by causing departures from classical tidal dynamics. The zonal mean vorticity ζ and Coriolis parameter f are given by the following equation:

$$\bar{\zeta} = \frac{-1}{a\cos\theta} * \frac{\partial(\bar{u}\cos\theta)}{\partial\theta} \quad (5)$$

$$\mathrm{f} = 2\Omega\sin\theta \quad (6)$$

$$\mathrm{R} = (-\bar{\zeta} + \mathrm{f})/\mathrm{f} \quad (7)$$

where a, $\bar{u}$ and θ correspond to the Earth radius, zonal mean zonal wind and latitude, respectively, and Ω is the Earth's rotation rate.

https://doi.org/10.5194/acp-2021-884
Preprint. Discussion started: 25 November 2021

In the classical theory, the vertically propagating DW1 is restricted near the equator due to the planet's rapid rotation. The ratio of the absolute and planetary vorticity R can be regarded as an enhancement of the Coriolis parameter f in the linearized tidal equations in a simple way. A larger R indicates that the latitudinal band becomes narrower (i.e., waveguide), where DW1 can propagate vertically (Wu et al., 2017). Conversely, a smaller ratio of R would benefit the upward propagation of DW1.

The MLR coefficient of R on Niño3.4 is illustrated in Figure 5. Below 50 km, the ratio R exhibits negative and positive responses to ENSO depending on different altitudes in the northern and southern subtropics. The R response to ENSO is positive at 55-100 km in the northern subtropics, and 65-85 km in the southern subtropics is positive. The increased ratio R in the mesosphere results in suppressed latitudinal band, which prevents the upward propagation of the DW1 tide during El Niño winters.

4.3 Effect of gravity wave forcing

In addition to tidal sources and tidal propagation, MLT tidal variability is also affected by interactions with GWs (Liu and Hagan, 1998; Li et al., 2009). GWs are the main driving force of MLT dynamic activity, which has an essential influence on tidal amplitude and phase (Walterscheid, 1981b; Lu et al., 2012; Liu et al., 2013). The effect of the GW forcing on tides is not fully understood due to the limited observation and lack of high-resolution model simulations that can fully resolve both tides and GWs. In WACCM, the GWs are parameterized, and their tropical sources are interactive and mainly triggered by convection in the tropics (Beres et al., 2005). Due to this source of interaction, the GW drag will likely be modulated by ENSO as the location and size of the ENSO-related convection change. The GW drag far away from the tropospheric source has a strong response to the wind. As mentioned above, we can determine the variation in the resistance of the convection-generated GW in the WACCM. We mainly focus on the latitudinal component of parameterized

https://doi.org/10.5194/acp-2021-884
Preprint. Discussion started: 25 November 2021

resistance because it is usually much larger than the meridional component (Yang et al. 2018).

To evaluate the effect of convection-generated GW forcing on the DW1 tide during DJF, the GW forcing needs to be projected into the time tendency of DW1-U. The phase of the DW1 tide time trend leads the tide by 6 hours; thus, the GW forcing can be calculated as follows:

$$GW_{\text{forcing}} = GW_{drag} * \cos(\omega * (\varphi_{GW} - (\varphi_U - 6))); \qquad (8)$$

where GW_{drag} is the GW drag, φ_{GW} and φ_{U} are the phases of DW1-GW and DW1-U, and ω （$\omega = 2\pi/24$） is the DW1 frequency.

The convection-generated DW1 GW forcing on the DW1 tide is positive in the southern subtropical upper mesosphere and negative below this tide (60–80 km) during the NH winter (Figure S3). In the NH, the DW1 GW forcing of the DW1 tide is positive in the subtropical mesosphere (15-35°N, 80-100 km) and negative in the tropical mesosphere (0-10°N, 80-100 km), indicating that convection-generated GW forcing will dampen the tides in the tropical MLT and enhance the tides in the NH and SH subtropical regions (Figure S3 and Figure S4). The linear regression coefficient of Niño3.4 in the GW forcing is significantly negative in the tropical MLT region (Figure 6, 80-100 km), suggesting that the decreased GW forcing would lead to a weaker DW1 U amplitude during El Niño winters.

Although parameterized GWs are excited by convection, it is difficult to find a direct cause and effect relationship between ENSO-related tropospheric changes and the GW-induced tidal forcing in the mesosphere. The GW forcing in the MLT not only depends on the generation of waves in the troposphere but also on zonal wind filtering when they propagate upward from the troposphere to the upper mesosphere. However, our study suggests that the ENSO modulation of tidal amplitude can come

https://doi.org/10.5194/acp-2021-884
Preprint. Discussion started: 25 November 2021

not only from the disturbance in tropospheric tidal sources and tidal propagation modulated by zonal wind but also from the disturbance of the GW-tidal interaction in the upper mesosphere.

5 Summary

The ENSO effects on the DW1 tide in the MLT region are investigated by using both satellite observations of temperature profiles and the SD-WACCM simulation. The DW1 amplitude of temperature observed by the SABER tends to decrease during the NH winter of 4 El Niño events from 2002 to 2020 when El Niño reaches its peak and increase during 3 La Niña events. In SD-WACCM simulations, the DW1 amplitude is suppressed during 7 of 8 El Niño winter (DJF) events from 1979 to 2014. The Hough (1,1) component dominates the MLT DW1-T variation, propagating vertically from 15 km to 100 km. The HR of the whole tropical troposphere (35°S-35°N, 0-16 km) decreased during El Niño peaks, corresponding to the suppressed DW1 tidal amplitude in the tropical troposphere.

ENSO modulates DW1 propagation by affecting the background wind field in the middle atmosphere. The ratio of the absolute and planetary vorticity $linearly$ affected by Niño3.4 is positive in the subtropical mesosphere, which suppresses the waveguide and thus the DW1 amplitude during El Niño winter. In addition, the GW forcing response to Niño3.4 is significantly negative in the tropical upper mesosphere, suppressing the MLT DW1 tide during El Niño winter.

https://doi.org/10.5194/acp-2021-884
Preprint. Discussion started: 25 November 2021

Atmospheric Chemistry and Physics Discussions

Data availability

SABER dataset are available at http://saber.gats-inc.com/data.php, ECMWF dataset used here are obtained at http://apps.ecmwf.int/datasets/data.

Author contributions

YC and CY designed the study, performed data analysis, prepared the figures and wrote the manuscript. TL initiated the study and contributed to supervision and interpretation. JY and JR contributed to editing the manuscript. XD contributed to interpretation. All authors contributed to discussion and interpretation.

Competing interests

The authors declare that they have no conflict of interest.

Acknowledgments

This work was funded by the National Natural Science Foundation of China grants (42130203, 41974175, 41874180), and the B-type Strategic Priority Program of the Chinese Academy of Sciences, Grant No. XDB41000000. JY and JMR's work is supported by the National Science Foundation grant AGS-1901126.

Reference

Beres, J. H., Garcia, R. R., Boville, B. A., & Sassi, F. (2005). Implementation of a gravity wave source spectrum parameterization dependent on the properties of convection in the Whole Atmosphere Community Climate Model (WACCM). *Journal of Geophysical Research*, 110, D10108. https://doi.org/10.1029/2004JD005504

Chapman, S., & Lindzen, R. S., *Atmospheric Tides*, 201 pp., D. Reidel, Norwell, Mass., 1970.

Davis, R. N., Du, J., Smith, A. K., Ward, W. E., & Mitchell, N. J. (2013). The diurnal and semidiurnal tides over Ascension Island (8°S, 14°W) and their interaction with the stratospheric QBO: Studies with meteor radar, eCMAM and WACCM. Atmospheric Chemistry and Physics, 13(18), 9543–9564. https://doi.org/10.5194/acp-13-9543-2013

Dhadly, M. S., Emmert, J. T., Drob, D. P., McCormack, J. P., & Niciejewski, R. (2018). Short-term and interannual variations of migrating diurnal and semidiurnal tides in the mesosphere and lower thermosphere. *Journal of Geophysical Research: Space Physics*, 123, 7106–7123. https://doi.org/10.1029/2018JA025748

Gan, Q., Du, J., Ward, W. E., Beagley., S. R., Fomichev., V. I., & Zhang, S. (2014). Climatology of the diurnal tides from eCMAM30 (1979 to 2010) and its comparisons with SABER. *Earth Planets Space 66*:103, https://doi.org/10.1186/1880-5981-66-103

Garcia-Herrera, R., N. Calvo, R. R. Garcia, and M. A. Giorgetta (2006), Propagation of ENSO temperature signals into the middle atmosphere: A comparison of two general circulation models and ERA-40 reanalysis data, *J. Geophys. Res.*, 111, D06101, https://doi.org/10.1029/2005JD006061.

Garcia, R. R., Marsh, D. R., Kinnison, D. E., Boville, B. A., & Sassi, F. (2007). Simulation of secular trends in the middle atmosphere, 1950–2003. *Journal of Geophysical Research, 112*, D09301. https://doi.org/10.1029/2006JD007485

https://doi.org/10.5194/acp-2021-884
Preprint. Discussion started: 25 November 2021

Atmospheric Chemistry and Physics Discussions

Gray, W. M., Atlantic seasonal hurricane frequency: Part I: El Nino and 30 mb quasi-biennial oscillation influences. *Mon. Wea. Rev.*, 112, 1649–1668, 1984 https://doi.org/10.1175/1520-0493(1984)112<1649:ASHFPI>2.0.CO;2

Gurubaran, S., & Rajaram, R. (1999). Long-term variability in the mesospheric tidal winds observed by MF radar over Tirunelveli (8.7°N, 77.8°E). *Geophysical Research Letters*, 26(8), 1113–1116. https://doi.org/10.1029/1999GL900171

Gurubaran, S., Rajaram, R., Nakamura, T., & Tsuda, T. (2005). Interannual variability of diurnal tide in the tropical mesopause region: a signature of the El Niño-Southern Oscillation (ENSO). *Geophysical Research Letters* 32(13): https://doi.org/10.1029/2005gl022928

Hagan, M.E., Burrage, M.D., Forbes, J.M. et al. (1999). QBO effects on the diurnal tide in the upper atmosphere. *Earth Planet Space*, 51, 571–578, doi:/10.1186/BF03353216

Hagan, M. E., Burrage, M. D., Forbes, J. M., Hackney, J., Randel, W. J., & Zhang, X. (1999). GSWM-98: Results for migrating solar tides. *Journal of Geophysical Research*, 104(A4), 6813–6827. https://doi.org/10.1029/1998JA900125

Hagan, M. E., and J. M. Forbes. (2002). Migrating and nonmigrating diurnal tides in the middle and upper atmosphere excited by tropospheric latent heat release, *J. Geophys. Res.*, *107*(D24), 4754, https://doi.org/10.1029/2001JD001236.

Hays, P. B., & Wu, D.L. (1994). Observations of the diurnal tide from space. *Journal of the Atmospheric Sciences*, *51*(20):3077–3093, https://doi.org/10.1175/1520-0469(1994)0512.0.Co;2

Hoerling, M. P., A. Kumar, and M. Zhong. (1997), El Niño, La Nina, and the nonlinearity of their teleconnections, *Journal of Climate*, 10, 1769–1786. https://doi.org/10.1175/1520-0442(1997)010<1769:ENOLNA>2.0.CO;2

Huang, F. T., Mayr, H. G., Reber, C. A., Russell, J., Mlynczak, M., & Mengel, J. (2006). Zonal-mean temperature variations inferred from SABER measurements on TIMED compared with UARS observations. *Journal of Geophysical Research: Atmospheres* 111(A10): https://doi.org/10.1029/2005ja011427

https://doi.org/10.5194/acp-2021-884
Preprint. Discussion started: 25 November 2021

Hurrell, J. W., Holland, M. M., Gent, P. R., Ghan, S., Kay, J. E., Kushner, P. J., et al. (2013). The Community Earth System Model: A framework for collaborative research. *Bulletin of the American Meteorological Society, 94(9)*, 1339-1360. https://doi.org/10.1175/BAMS-D-12-00121.1

Kunz, A., Pan, L., Konopka, P., Kinnison, D., & Tilmes, S. (2011). Chemical and dynamical discontinuity at the extratropical tropopause based on START08 and WACCM analyses. *Journal of Geophysical Research, 116*, D24302. https://doi.org/10.1029/2011JD016686

Masaru Kogure, Huixin Liu (2021). DW1 Tidal Enhancements in the equatorial MLT during 2015 El Niño: The relative role of tidal heating and propagation. *Journal of Geophysical Research,* https://doi.org/10.1029/2021JA029342.

Lieberman, R. S., Ortland, D. A., & Yarosh, E. S. (2003). Climatology and interannual variability of diurnal water vapor heating. Journal of Geophysical Research: Atmospheres 108(D3): https://doi.org/10.1029/2002jd002308

Lieberman, R. S., Riggin, D. M., Ortland, D. A., Nesbitt, S. W., & Vincent, R. A. (2007). Variability of mesospheric diurnal tides and tropospheric diurnal heating during 1997–1998. Journal of Geophysical Research: Atmospheres 112(D20): https://doi.org/10.1029/2007jd008578

Lindzen, R. S., and S. Chapman (1969), Atmospheric tides, *Space Science Review*, 10(1), 3–188

Li, T., She, C. -Y., Liu, H., Yue, J., Nakamura, T., Krueger, D. A., et al. (2009). Observation of local tidal variability and instability, along with dissipation of diurnal tidal harmonics in the mesopause region over Fort Collins, Colorado (41°N, 105°W). *Journal of Geophysical Research: Atmospheres (1984–2012)*, *114*(D6). https://doi.org/10.1029/2008jd011089

Li, T., Calvo, N., Yue, J., Dou, X., Russell III, J. M., Mlynczak, M. G., She, C.-Y., & Xue, X. (2013). Inflfluence of El Niño-Southern Oscillation in the mesosphere. *Geophysical Research Letters*, 40, 3292–3296, https://doi.org/10.1002/grl.50598.

https://doi.org/10.5194/acp-2021-884
Preprint. Discussion started: 25 November 2021

Li, T., Calvo, N., Yue, J., Russell, J. M. I., Smith, A. K., Mlynczak, M. G., Chandran, A., Dou, X., & Liu, A. Z. (2016). Southern Hemisphere summer mesopause responses to El Niño-Southern Oscillation. *Journal of Climate*, 29(17), 6319– 6328. https://DOI.org/10.1175/JCLI-D-15-0816.1

Liu, A. Z., Lu, X., & Franke, S. J. (2013). Diurnal variation of gravity wave momentum flflux and its forcing on the diurnal tide. *Journal of Geophysical Research – Atmospheres*, 118, 1668–1678. https://doi.org/10.1029/2012JD018653

Liu, H., Sun, Y.-Y., Miyoshi, Y., & Jin, H. (2017). ENSO effffects on MLT diurnal tides: A 21 year reanalysis data-driven GAIA model simulation. *Journal of Geophysical Research: Space Physics*, 122, 5539–5549, https://doi.org/10.1002/2017JA024011.

Liu, H.-L., Wang, W., Richmond, A. D., & Roble, R. G. (2010). Ionospheric variability due to planetary waves and tides for solar minimum conditions. *Journal of Geophysical Research: Space Physics*, *115*, A00G01, https://doi.org/10.1029/2009JA015188.

Liu, H.-L., & Hagan, M. E. (1998). Local heating/cooling of the mesosphere due to gravity wave and tidal coupling. *Geophysical Research Letters*, *25*, 2941–2944 https://doi.org/10.1029/98GL02153

Lu, X., Liu, A. Z., Swenson, G. R., Li, T., Leblanc, T., & McDermid, I. S. (2009). Gravity wave propagation and dissipation from the stratosphere to the lower thermosphere. Journal of Geophysical Research: Atmospheres, 114, D11101, https://doi.org/10.1029/2008JD010112.

Lu, X., Liu, H.-L., Liu, A. Z., Yue, J., McInerney, J. M., & Li, Z. (2012). Momentum budget of the migrating diurnal tide in the Whole Atmosphere Community Climate Model at vernal equinox. *Journal of Geophysical Research*, 117, D07112. https://doi.org/10.1029/2011JD017089

Lu, X., Liu, A. Z., Oberheide, J., Wu, Q., Li, T., Li, Z., et al. (2011). Seasonal variability of the diurnal tide in the mesosphere and lower thermosphere over Maui, Hawaii (20.7°N, 156.3°W). *Journal of Geophysical Research, 116*, D17103. https://doi.org/10.1029/2011JD015599

Mayr H.G., Mengel J.G. (2005). Interannual variations of the diurnal tide in the mesosphere generated by the quasi-biennial oscillation, *J Geophys Res 110:D10111.* doi:10.1029/2004JD005055

McLandress, C., Shepherd, G. G., & Solheim, B. H. (1996). Satellite observations of thermospheric tides: Results from the wind imaging interferometer on UARS. *Journal of Geophysical Research: Atmospheres 101*(D2):4093–4114, https://doi.org/10.1029/95jd03359

McLandress, C. (2002). Interannual variations of the diurnal tide in the mesosphere induced by a zonal- mean wind oscillation in the tropics, *Geophys. Res. Lett*., 29(9), doi:10.1029/2001GL014551.

Mertens, C. J., Mlynczak, M. G., Lopez-Puertas, M., Wintersteiner, P. P., Picard, R. H., Winick, J. R., & Gordley, L. L. (2001). Retrieval of mesospheric and lower thermos pheric kinetic temperature form measurements of CO2 15 μm Earth limb emission under non-LTE conditions, *Geophysical Research Letters*, 28(7), 1391-1394. https://doi.org/10.1029/2000GL012189

Mertens, C. J., Schmidlin, F. J., Goldberg, R. A., Remsberg, E. E., Pesnell, W. D., Russell, J. M., Mlynczak, M. G., Lopez-Puertas, M., Wintersteiner, P. P., Picard, R. H., Winick, J. R., & Gordley, L. L. (2004). SABER observations of mesospheric temperatures and comparisons with falling sphere measurements taken during the 2002 summer MaCWAVE campaign. *Geophysical Research Letters 31*(3). https://doi.org/10.1029/2003gl018605

Oberheide, J., Forbes, J. M., Zhang, X., & Bruinsma, S. L. (2011). Climatology of upward propagating diurnal and semidiurnal tides in the thermosphere. *Journal of Geophysical Research: Space Physics*, *116*, A11306. https://doi.org/10.1029/2011JA016784

https://doi.org/10.5194/acp-2021-884
Preprint. Discussion started: 25 November 2021

Atmospheric Chemistry and Physics Discussions

Pedatella, N. M., & Liu, H. L. (2012). Tidal variability in the mesosphere and lower thermosphere due to the El Niño-Southern Oscillation. *Geophysical Research Letters 39*. https://doi.org/10.1029/2012gl053383

Pedatella, N. M., & Liu, H. L. (2013). Influence of the El Niño Southern Oscillation on the middle and upper atmosphere. *Journal of Geophysical Research:* Atmospheres 118(5):2744–2755, https://doi.org/10.1002/Jgra.50286

Ramesh, K., Smith, A. K., Garcia, R. R., Marsh, D. R., Sridharan, S., & Kishore Kumar, K. (2020). Long-term variability and tendencies in migrating diurnal tide from WACCM6 simulations during 1850–2014. *Journal of Geophysical Research: Atmospheres*, 125, e2020JD033644. https://doi.org/10.1029/2020JD033644

Randel, W. J. , Shine, K. P. , Austin, J. , Barnett, J. , Claud, C. , & Gillett, N. P. , et al. (2009). An update of observed stratospheric temperature trends. *Journal of Geophysical Research: Atmospheres*. 114, D02107, https://doi.org/10.1029/2008JD010421

Rezac, L., Y. Jian, J. Yue, J. M. Russell III, A. Kutepov, R. Garcia, K. Walker, and P. Bernath (2015), Validation of the global distribution of CO2 volume mixing ratio in the mesosphere and lower thermosphere from SABER, *J. Geophys. Res. Atmos.*, 120, 12,067– 12,081. https://doi.org/10.1002/2015JD023955.

Smith, A. K. (2012). Global Dynamics of the MLT. *Surveys in Geophysics,* 33(6): 1177–1230, https://doi.org/10.1007/s10712-012-9196-9

Sun, Y. Y., Liu, H., Miyoshi, Y., Liu, L., Chang, L. C. (2018). El Niño-Southern Oscillation effect on quasi-biennial oscillations of temperature diurnal tides in the mesosphere and lower thermosphere. Earth Planets Space. https://doi.org/10.1186/s40623-018-0832-6

Vincent, R. A., Kovalam, S., Fritts, D. C., & Isler, J. R. (1998). Long-term MF radar observations of solar tides in the low-latitude mesosphere: Interannual variability and comparisons with GSWM. *Journal of Geophysical Research*, 103(D8), 8667–8683. https://doi.org/10.1029/98JD00482

https://doi.org/10.5194/acp-2021-884
Preprint. Discussion started: 25 November 2021

Atmospheric Chemistry and Physics Discussions

Volland & Hans. *Atmospheric Tidal and Planetary Waves*[M]. Springer Netherlands, 1988

Wallace J. M. , & Hobbs P. V., *Atmospheric science, 2006*

Wallace, J. M., Panetta. R. L., & J. Estberg (1993). Representation of the equatorial quasi-biennial oscillation in EOF phase space. *Journal of the Atmospheric Sciences*, *50*, 1751 – 1762, https://doi.org/10.1175/1520-0469(1993)050<1751:ROTESQ>2.0.CO;2.

Walterscheid, R. L. (1981a). Inertia-gravity wave induced accelerations of mean flow having an imposed periodic component: Implications for tidal observations in the meteor region. Journal of Geophysical Research: Atmospheres, 86, 9698 – 9706. https://doi.org/10.1029/JC086iC10p09698

Walterscheid, R. L. (1981b). Dynamical cooling induced by dissipating internal gravity waves. Geophysical Research Letters, 8(12), 1235 – 1238. https://doi.org/10.1029/GL008i012-p01235

Warner, K., Oberheide, J. (2014) Nonmigrating tidal heating and MLT tidal wind variability due to the El Niño-Southern Oscillation. *Journal of Geophysical Research: Atmospheres 119*:1249–1265. https://doi.org/10.1002/2013JD020407

Xu, J. Y., Liu, H. L., Yuan, W., Smith, A. K., Roble, R. G., Mertens, C. J., Russell, J. M., & Mlynczak, M. G. (2007a). Mesopause structure from thermosphere, ionosphere, mesosphere, energetics, and dynamics (TIMED)/sounding of the atmosphere using broadband emission radiometry (SABER) observations. *Journal of Geophysical Research: Atmospheres 112* (D9). https://doi.org/10.1029/2006jd007711

Xu, J. Y., Smith, A. K., Yuan, W., Liu, H. L., Wu, Q., Mlynczak, M. G., Russell, J. M. (2007b). Global structure and long-term variations of zonal mean temperature observed by TIMED/SABER. *Journal of Geophysical Research: Atmospheres*, 112, D24106: https://doi.org/10.1029/2007jd008546

Xu, J., A. K. Smith, H.-L. Liu, W. Yuan, Q. Wu, G. Jiang, M. G. Mlynczak, J. M. Russell III, and S. J. Franke (2009), Seasonal and quasi-biennial variations in the migrating diurnal tide observed by Thermosphere, Ionosphere, Mesosphere, Energetics and Dynamics (TIMED), *J. Geophys. Res.*, 114, D13107, doi:10.1029/2008JD011298.

Yang, C., Li, T., Dou, X., & Xue, X. (2015). Signal of central Pacific El Niño in the Southern Hemispheric stratosphere during Austral spring. *Journal of Geophysical Research: Atmospheres*, *120*,11,438–11,450. https://doi.org/10.1002/ 2015JD023486.

Yang, C., Smith, A. K., Li, T., & Dou, X. (2018). The effect of the Madden-Julian oscillation on the mesospheric migrating diurnal tide: A study using SD-WACCM. *Geophysical Research Letters, 45*, 5105–5114. https://doi.org/10.1029/2018GL077956

Zhang, X., Forbes, J. M., & Hagan, M. E. (2010). Longitudinal variation of tides in the MLT region: 1. Tides driven by tropospheric net radiative heating. *Journal of Geophysical Research: Space Physics* , *115*, A06316, https://doi.org/10.1029/2009JA014897.

Zhou, X., Wan, W., Yu, Y., Ning, B., Hu, L., and Yue, X. (2018). New approach to estimate tidal climatology from ground-and space-based observations. *Journal of Geophysical Research: Space Physics, 123, 5087– 5101*. doi:10.1029/2017JA024967

https://doi.org/10.5194/acp-2021-884
Preprint. Discussion started: 25 November 2021

Atmospheric Chemistry and Physics Discussions

Table 1. The list of ENSO years with corresponding Niño3.4 indices and anomaly DW1 temperature amplitudes of the SD-WACCM simulations averaged over 10°S-10°N at 100 km.

El Niño events	Niño3.4 index	SD-WACCM anomalous DW1 T AMP (K)
1982-1983	2.14	-0.22
1986-1987	1.11	-2.90
1991-1992	1.69	-1.56
1994-1995	1.22	1.56
1997-1998	2.33	-1.87
2002-2003	1.37	-0.55
2006-2007	1.09	-1.30
2009-2010	1.43	-1.82
AVG	1.54	-0.96

Table 2. The correlation coefficient between the DW1 T amplitude at 15 km and the mass-weighted HR in different areas during the winters of 1979-2014. The bold numbers indicate that the correlation coefficients are significant at the 95% level. The MLR coefficient on the normalized Niño3.4 index (10^{-3} mw m^{-3} $index^{-1}$) is also exhibited.

Altitude and latitude ranges	0-16 km, 35°N-35°S)	0-12 km, 35°N-35°S)	5-10 km, 35°N-35°S)	5-10 km,20° N-20°S)
Correlation coefficient	**0.45**	**0.36**	0.32	0.32
MLR coefficient on Niño3.4	-3	-10	-26	-9

https://doi.org/10.5194/acp-2021-884
Preprint. Discussion started: 25 November 2021

Figure captions

Figure 1. (a) The residual DW1 temperature amplitude of SABER observations averaged over 10°S-10°N at 100 km during 2002-2021. (b) Same as in (a) but for SD-WACCCM. (c) Niño3.4 index. Dashed lines represent ENSO events. The red and blue arrows denote the El Niño and La Niña events, respectively.

Figure 2. The linear regression coefficient of normalized Niño3.4 in SABER (a) and SD-WACCM (b) DW1-T. The contour interval is 0.2 K for SABER and 0.1 K for SD-WACCM. Red represents a positive response, and blue represents a negative response; the grey regions denote confidence levels below 95% for the F test.

Figure 3. (a) The red line indicates the anomalous DW1 temperature amplitude of SD-WACCM simulations averaged over 10°S-10°N at 100 km during the 1979-2013 winter (DJF). The blue line indicates the Hough (1,1) mode of the DW1 temperature amplitude residual at 100 km during the 1979-2013 winter (DJF). (b) The thin black line indicates the Hough (1,1) DW1-T phase of SD-WACCM simulations at 0-100 km during the 1979-2013 winter (DJF). The thick black horizontal line indicates the standard deviation of the DW1-T phase. The red line is the same but for El Niño winter. (c) The blue line is the same as in (a), and the black line is the same but for 15 km.

Figure 4. The linear regression coefficient of normalized Niño3.4 in SD-WACCM heating amplitude (mW/m^3 per index) during 1979-2013 winters (DJF). Red represents a positive response, and blue represents a negative response; the grey regions denote confidence levels below 95% according to the F test.

Figure 5. The anomaly of the ratio of the absolute and planetary vorticity, δR. The thick, solid red and blue lines denote the averages of the Northern Hemisphere (from 15°N to 30°N) and Southern Hemisphere (from 15°S to 30°S), respectively.

Figure 6. The linear regression coefficient of normalized Niño3.4 in the GW forcing on the amplitude of DW1-U during 1979-2013 winters (DJF). Red represents a positive response, and blue represents a negative response; the grey regions denote confidence levels below 95%.

681 **Figures**

682

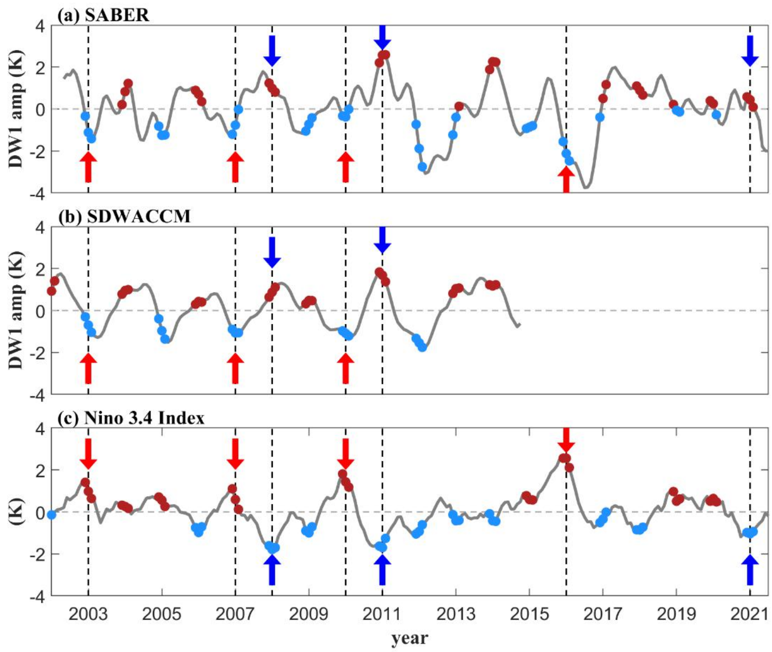

683

684 **Figure 1.** (a) The residual DW1 temperature amplitude of SABER observations averaged over

685 10°S-10°N at 100 km during 2002-2021. (b) Same as in (a) but for SD-WACCCM. (c) Niño3.4

686 index. Dashed lines represent ENSO events. The red and blue arrows denote the El Niño and La

687 Niña events, respectively.

688

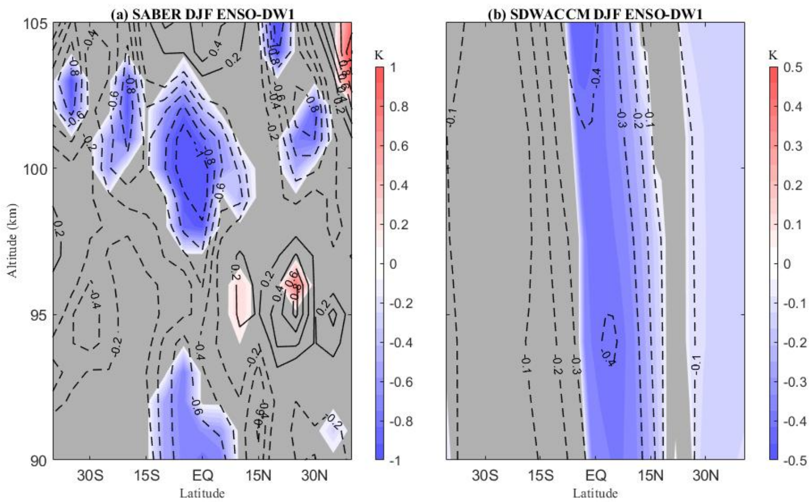

Figure 2. The linear regression coefficient of normalized Niño3.4 in SABER (a) and SD-WACCM (b) DW1-T. The contour interval is 0.2 K for SABER and 0.1 K for SD-WACCM. Red represents a positive response, and blue represents a negative response; the grey regions denote confidence levels below 95% for the F test.

https://doi.org/10.5194/acp-2021-884
Preprint. Discussion started: 25 November 2021

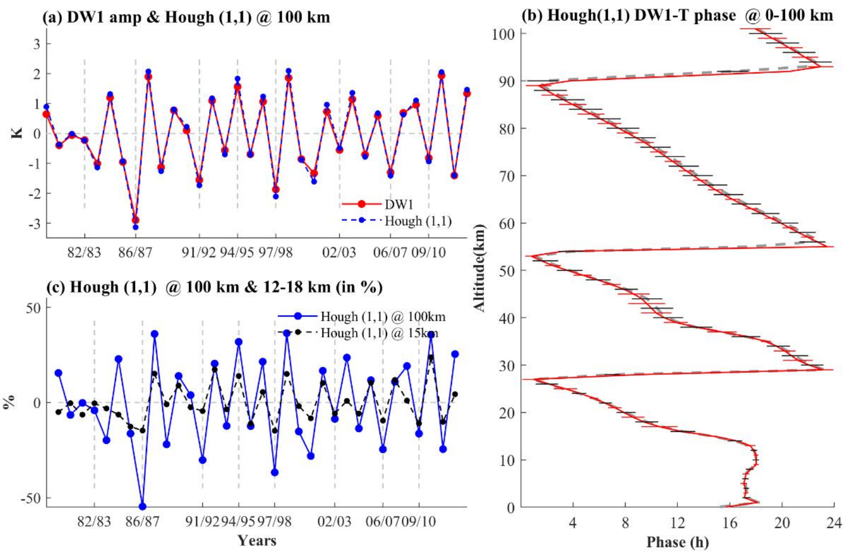

Figure 3. (a) The red line indicates the anomalous DW1 temperature amplitude of SD-WACCM simulations averaged over 10°S-10°N at 100 km during the 1979-2013 winter (DJF). The blue line indicates the Hough (1,1) mode of the DW1 temperature amplitude residual at 100 km during the 1979-2013 winter (DJF). (b) The thin black line indicates the Hough (1,1) DW1-T phase of SD-WACCM simulations at 0-100 km during the 1979-2013 winter (DJF). The thick black horizontal line indicates the standard deviation of the DW1-T phase. The red line is the same but for El Niño winter. (c) The blue line is the same as in (a), and the black line is the same but for 15 km.

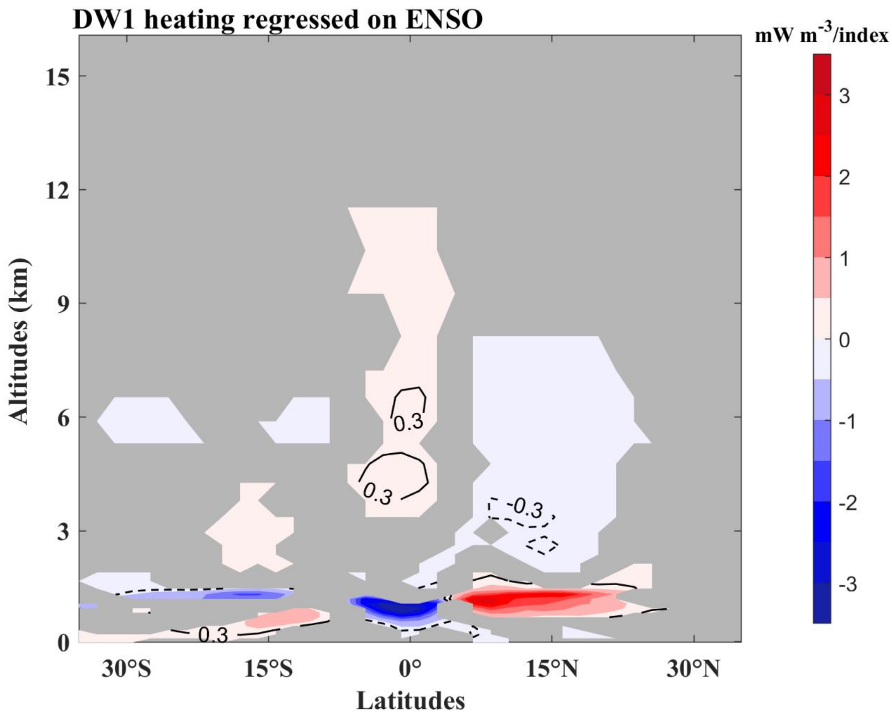

Figure 4. The linear regression coefficient of normalized Niño3.4 in SD-WACCM heating amplitude (mW/m^3 per index) during 1979-2013 winters (DJF). Red represents a positive response, and blue represents a negative response; the grey regions denote confidence levels below 95% according to the F test.

https://doi.org/10.5194/acp-2021-884
Preprint. Discussion started: 25 November 2021

716 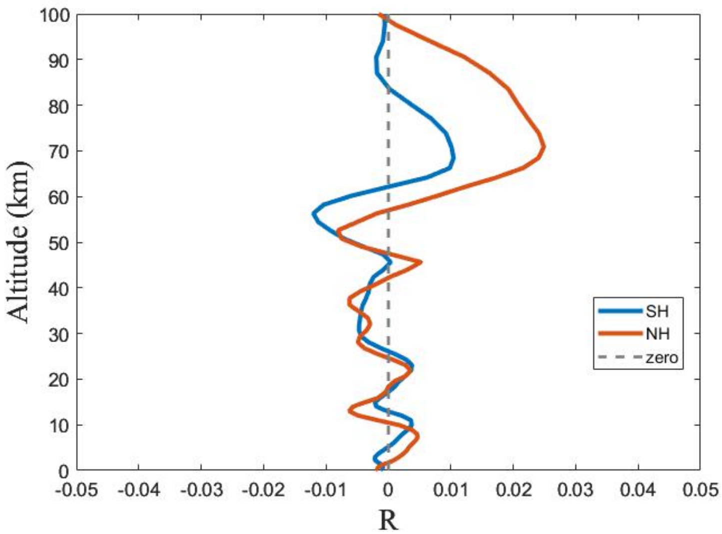

717 **Figure 5**. The anomaly of the ratio of the absolute and planetary vorticity, δR. The thick, solid red
718 and blue lines denote the averages of the Northern Hemisphere (from 15°N to 30°N) and Southern
719 Hemisphere (from 15°S to 30°S), respectively.
720

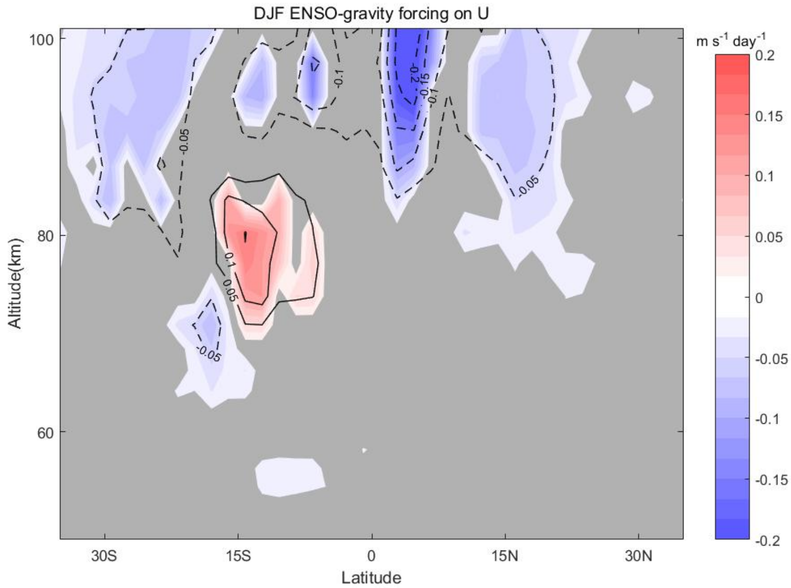

721

722 **Figure 6**. The linear regression coefficient of normalized Niño3.4 in the GW forcing on the

723 amplitude of DW1-U during 1979-2013 winters (DJF). Red represents a positive response, and

724 blue represents a negative response; the grey regions denote confidence levels below 95%.

725